Materials Advances

ROYAL SOCIETY OF CHEMISTRY

PAPER

View Article Online
View Journal | View Issue

Cite this: *Mater. Adv.*, 2022, 3, 9071

Upcycling of waste jute biomass to advanced biocarbon materials: the effect of pyrolysis temperature on their physicochemical and electrical properties†

Neelima Tripathi, [ab] Arturo Rodriguez Uribe, [ab] Haftom Weldekidan, [ab] Manjusri Misra [ab] and Amar K. Mohanty *[ab]

In this work, waste burlap (jute) biomass from the coffee industry was valorized to synthesize advanced biocarbon. Waste burlap biomass was carbonized at various temperatures (325, 350, 400, 500, 600, 700, 800, 900 and 1000 °C), followed by ball-milling. The pyrolysis yield, functionality, particle size, surface area, interlayer *d*-spacing, ash content, thermal stability, carbon/oxygen content, graphitic content and electrical conductivity of the biocarbon obtained after each carbonization were determined. With an increase in the carbonization temperature a decrease in yield occurred. The yield of biocarbon obtained at 325 °C was noted to be ~71 wt%, which decreased with an increase in the carbonization temperature and remained ~22 wt% from 800–1000 °C. It was observed that the functional groups of the carbonized biomass (biocarbon) due to the presence of cellulose, hemicellulose and lignin in biomass were retained up to ~600 °C and diminished at higher pyrolysis temperatures. In addition, among 325–1000 °C carbonization temperatures, the highest thermally stable biocarbon and highest carbon content (85%) were obtained after pyrolyzing burlap biomass at 1000 °C. XRD analysis revealed the reduction in *d*-spacing as the carbonization temperature increases leading to close packing of layers. Importantly, burlap biocarbon (pyrolyzed at ~1000 °C, compressed at 1.12 MPa) showed significant enhancement in electrical conductivity (~3.5 times higher) than commercial graphite. The research has demonstrated that the synthesized sustainable biocarbon can be further upcycled. High temperature (~1000 °C) pyrolyzed biocarbon has the potential to be used as biographite and can substitute fossil fuel-derived for certain semi-conductive materials.

Received 13th June 2022,
Accepted 9th October 2022

DOI: 10.1039/d2ma00678b

rsc.li/materials-advances

1. Introduction

Conventional carbon products for instance graphite, graphene, carbon black, and carbon fibers are used immensely in day-to-day life products and applications such as batteries[1] and automotive composites,[2] water desalination,[3] biomedical[4] and construction industries.[5] These materials are derived from fossil-fuel based precursors[6] such as pitch, benzene, toluene, coal, coal tar, asphalt and hydrocarbons (gaseous form). Thus, the extensive usage of fossil-fuel-based resources results in the depletion of non-renewable resources, increasing oil prices and greenhouse gas emissions.[7]

Conventional fossil fuel-based carbon can be replaced with under-valued biobased carbon (biocarbon). Biocarbon/biochar, generally developed by carbonization of renewable (waste agricultural feedstocks) resources, is a low-cost sustainable alternative that helps in carbon sequestration.[7] The final cost of biocarbon depends on the feedstock source, carbonization unit type, coproducts obtained other than biocarbon, and market demand.[8] Researchers investigated that the production cost of biocarbon from yard waste can be as low as USD 51 per ton. Further, the greenhouse gas emissions balance of biocarbon (from dried biomass) production and application can be as low as −1054 kg CO_2e per ton.[9] In comparison with fillers such as glass fibers used for making biocomposites, biocarbon is 70% less expensive.[10]

This upcycled waste biomass in the biocarbon form with respect to natural fibers is more chemically and thermally stable, is hydrophobic and has a wide processing window, unlike natural fibers (the degradation temperature of natural fibers starts at >200 °C).[11] It has been explored that biocarbon

[a] *Bioproducts Discovery and Development Centre, Department of Plant Agriculture, Crop Science Building, University of Guelph, Guelph, Ontario N1G 2W1, Canada. E-mail: mohanty@uoguelph.ca*
[b] *School of Engineering, Thornborough Building, University of Guelph, Guelph, Ontario N1G 2W1, Canada*

† Electronic supplementary information (ESI) available. See DOI: https://doi.org/10.1039/d2ma00678b

as a filler significantly enhances the performance of a polymer matrix with increased sustainable content and has the potential to be used as a next-generation carbon material.[12] The research towards developing biobased, economically viable and sustainable composite[13] injection molded parts will create a niche market for agro-waste biomass.

The thermochemical conversion of biomass to biocarbon in an inert or limited oxygen environment *via* carbonization is a waste management technique that increases bioeconomy and the potential to develop value-added applications. During the process, decomposition or breakdown of the material occurs with an increase in temperature. Other products that are obtained with char or biocarbon (solid form) are bio-oil (liquid form that can also be valorized[14,15]) and syngas (gaseous form, a mixture of carbon monoxide and hydrogen) or pyro-gas (gaseous). The reactions that primarily occur during the process are dehydration, recondensation, decarboxylation and aromatization.

Pyrolysis at low temperatures (torrefaction) and that at high temperatures are carbonization processes in which a thermally stable carbon-rich solid product is obtained. According to Chang *et al.*[16] a slow pyrolysis rate (<10 °C min^{-1}) results in a high biocarbon yield. However, a fast pyrolysis rate ($\sim$100 °C min^{-1} or more) is favorable for producing the bio-oil.

The physicochemical properties, such as yield, carbon content, ash content, maximum degradation temperature, porosity, surface area, hydrophobicity, distance between planes of atoms (*d*-spacing) and graphitization, of the biocarbon from different feedstocks depend on (i) the primary molecular structure of the selected feedstock; (ii) composition of biomass (percent of cellulose, hemicellulose and lignin present); (iii) heating rate during carbonization; (iv) carbonization temperature; (v) carbonization retention/residence time; (vi) physical or chemical treatments conducted on the biomass preceding carbonization.

However, extensive research is still needed to enhance the commercial value of biocarbon exponentially. Based on its characteristic properties, biocarbon shows incredible scope to be used for the upcycling technology for sustainable development. Adesemuyi *et al.*[17] studied the effects of pyrolysis temperatures of 400 and 600 °C on elephant grass and confirmed that it could remove nitrate ions from water. You *et al.*[7] prepared activated *Miscanthus* biocarbon as an electrode material for developing an electric double-layer capacitor. The biocarbon was activated using potassium hydroxide, which increased the surface area. The effects of pyrolysis temperature on biomasses such as sugarcane bagasse,[18] corn straw,[19] rapeseed stems,[20] hazelnut shells,[21] distillers' dried grains with solubles (DDGS)[22] and sawdust[23] have been explored.

Among the various renewable biomasses, waste burlap (jute) biomass is less probed and still needs attention as it is an unexplored agro-waste having unique physical and chemical properties. Jute biomass is composed of cellulose ($\sim$55–75%), hemicellulose ($\sim$12–20%), lignin ($\sim$12–17%) (comparatively stable, primarily aromatic and the molecular structure varies among biomass[24]), pectin and some waxy materials.[25] Jute fibers are one of the low-cost bast fibers among kenaf, sisal, hemp and flax. Jute has a specific heat value of 1360 J kg K^{-1}.[26] The degree of polymerization of untreated jute fibers was found to be 403.[27] The easy availability, poor spinnability and rough touch make it an undervalued industrial fabric.[28] Jute bags/sacks/fabrics are extensively used in various sectors, namely fertilizers, cement, agriculture, chemicals and transportation. However, the mass production of this inexpensive packaging material is gaining environmental concerns and needs disposal management.[29] In addition, burlap (jute) bags are used to pack coffee beans, which are often reused to pack other products such as vegetables (such as potatoes) and grains and used for gardening. However, based on the calculation, it was predicted that only the coffee industry in Canada could produce about $\sim$1899.8 tons of burlap waste if not reused.

In this study, used burlap (strong, coarsely woven fibers) bags made of jute fibers produced as waste from the coffee industry were used to prepare sustainable burlap biocarbon samples. Jute is mainly composed of cellulose, hemicellulose and lignin[30,31] and was pyrolyzed from 325 to 1000 °C. Physicochemical properties such as the yield, surface area, spacing between biocarbon layers, ash content, functionality, carbon content, graphitic content and evolution of residual gaseous components from biocarbon with a rise in the carbonization temperature were determined. Furthermore, the electrical conductivity of biocarbon with an increase in the compression load was also measured.

2. Experimental

2.1 Materials

Waste burlap bags that were used for storing green (unroasted) coffee beans were kindly provided by Club Coffee, Ontario, Canada. Commercial graphite (Model-299, Beijing Great Wall Co. Ltd) was used to compare a few of the critical results of the prepared biocarbon in the laboratory.

2.2 Methods

2.2.1. Ground Burlap Fiber (GBF) preparation. A piece of burlap bags was milled using a Retsch ZM 200 (centrifugal) vortex mill (Verder Scientific, Haan Germany) at 6000 rpm using a ring sieve of 0.08 mm to obtain fine burlap fibers (BF) that were used for investigating and comparing its properties with biocarbon.

2.2.2. Burlap biomass carbonization (325–1000 °C biocarbon preparation). Before pyrolysis of burlap bags, the bags consisting of stitched borders by plastic strings were removed, and the bags were dried in an oven (hot-air) at 80 °C for 24 h. Pyrolysis was conducted using a Carbolite Gero pyrolyzer (OPTI-TECH, model GLO 10/11-1G), and a maximum temperature of up to 1100 °C can be reached. The dried bags ($\sim$1000 g) were then pyrolyzed at 325 to 1000 °C at 5 °C min^{-1} (ramp rate). The dwell or retention time maintained for pyrolysis was 90 min for temperatures 325–800 °C. At higher temperatures, 900 and 1000 °C, the retention time maintained was 60 and 45 min.,

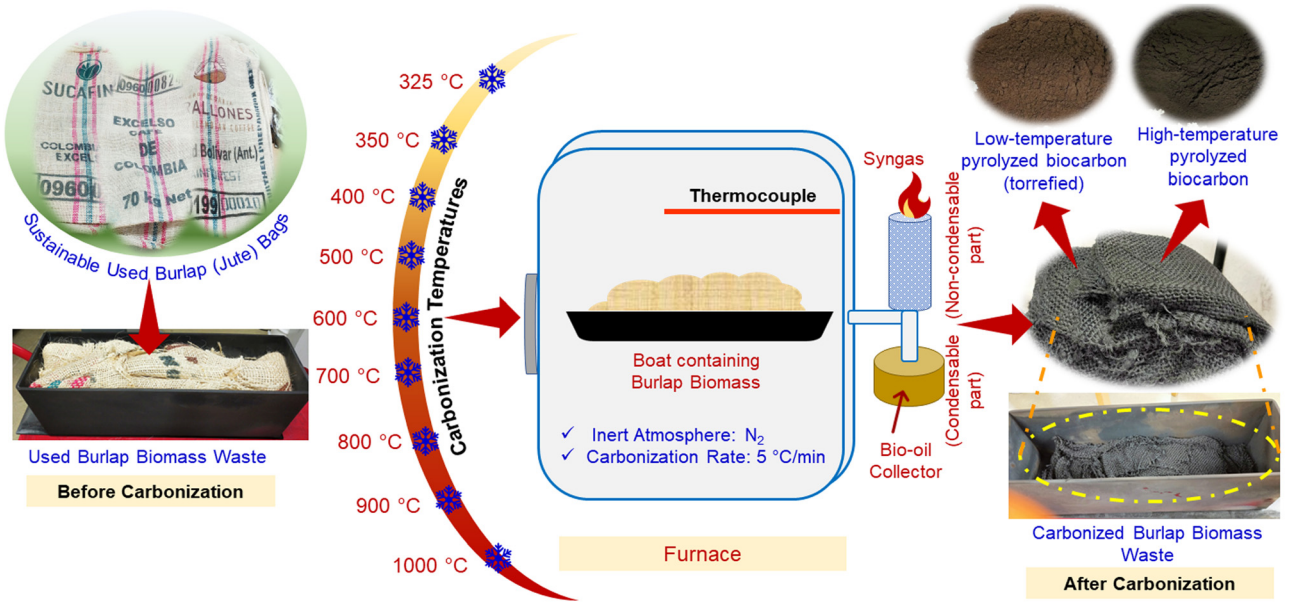

Fig. 1 Schematic illustration of the carbonization process conducted to prepare burlap biocarbon.

respectively. During the pyrolysis, nitrogen gas was purged at 60 L h^{-1} till the temperature of the pyrolyzer reached room temperature. A schematic representation of the carbonization process is shown in Fig. 1.

2.2.3. Ball milling of the burlap biocarbon. After pyrolysis, the carbonized samples (325–1000 °C) were milled using a blender (Nutri Ninja). The samples were sieved using a 500 μm mesh size screen to check if no coarser particles were present in the biocarbon samples. Furthermore, the burlap biocarbon samples carbonized at various temperatures were ball milled at 200 rpm using a Fritsch Pulverisette 5 (Fritsch GmbH, Germany) with zirconium dioxide grinding balls (1 cm diameter) for one hour with counter-rotation.

2.3 Characterization

2.3.1 Burlap biocarbon yield. After each pyrolysis, the biocarbon yield was obtained using eqn (1):

$$\text{Yield (\%)} = (W_{BioC}/W_0) \times 100 \quad (1)$$

where W_{BioC} is the weight (g) of the biocarbon after carbonization and W_0 is the weight (g) of the burlap biomass prior to carbonization (the moisture content (%) present in the burlap biomass before carbonization was reduced from its original weight). The initial (before carbonization) moisture content of the burlap biomass was checked using a moisture analyser (model MA37-1, Sartorius).

2.3.2 FTIR. Attenuated total reflectance (ATR)-Fourier transform infrared (FTIR) spectra of the GBF and burlap biocarbon carbonized at various temperatures were collected using a Nicolet 6700 spectrometer from ThermoFisher Scientific (Waltham, Massachusetts, USA). The samples were investigated at 256 scans per sample and 4 cm^{-1} resolution.

2.3.3 Thermogravimetric analysis (TGA) and the ash content. TGA was conducted using TA Q500 (TA Instruments, USA) to check the thermal stability of the GBF and the carbonized biocarbon samples. The weight of the samples taken for analysis was 7–10 mg. The analysis was conducted under an N_2 atmosphere at 10 °C min^{-1} to 800 °C (maximum instrument limit for the analysis). The ash content of the samples was determined using ASTM E1131-08. Air was flushed into the TGA furnace at 800 °C, and the temperature was maintained for 20 min. The analysis for determining the ash content was repeated twice, and the average with standard deviation was obtained.

2.3.4 TGA-FTIR. The thermogravimetric analysis (TGA) and Fourier Transform Infrared Spectroscopy (FTIR) were performed using a 5500, TA Instruments, thermogravimetric analyzer (USA) and a Thermo Scientific Nicolet iS20 FTIR spectrometer (USA), respectively. TA TRIOS software was used to operate the TGA instrument, and OMNIC was used to operate the FTIR instrument. The inert atmosphere was maintained throughout the analysis by maintaining a 50 mL min^{-1} nitrogen gas flow rate. The dried biocarbon samples were heated at 20 °C min^{-1} (ramp rate) from 30 to 900 °C. Each carbonized biocarbon was analyzed for 6 scans and 8 cm^{-1} resolution.

2.3.5 Raman spectroscopy. The Raman spectra were acquired using a ThermoFisher Scientific DXR™2 microscope (Waltham, MA, USA). The wavelength and power of the laser set for analysis were 532 nm and 2 mW, respectively, for excitation using a 10× objective lens. The total number of scans per sample was set as 128 for a 4.0 s exposure time. The Origin software was used to determine the best fit peak by Gaussian function at Raman shift at the D band (1300–1400 cm^{-1}) and the G band (1500–1600 cm^{-1}). Four-peak fitting was done to best fit the spectra for each sample. The ratio of the intensities (I_D/I_G) in accordance with the amplitude height of these deconvoluted peaks was determined. Raman analysis was conducted only for 500–1000 °C, as lower pyrolyzed samples were not suitable for the laser power.

2.3.6 Brunauer–Emmett–Teller (BET) analysis. The surface area of the burlap biocarbon samples was determined using a BET analyser Autosorb-iQ (Quantachrome Instruments, USA) and using ASiQwin 5 software. Calibration was conducted using helium gas. Nitrogen gas adsorbed on the samples was used to determine the surface area. The ball milled biocarbon samples (~300 mg) were weighed in bulb cells (6 mm). Degassing was performed at 200 °C at 15 °C min^{-1} with an outgas (soak) time of 180 min. The analysis was conducted using liquid N_2 as a coolant. In the volume to relative pressure curve, the linear region was selected over a P/P_0 range (0.05–0.35) according to the ASTM standard D6556-10.

2.3.7 SEM-EDS. Scanning electron microscopy (SEM) in conjugation with energy-dispersive X-ray spectroscopy (EDS) was performed using a Phenom ProX microscope (Netherlands). The micrographs were acquired, and the elemental (carbon (C) and oxygen (O_2)) composition was determined for the synthesized biocarbon samples at 1300× magnification at an acceleration voltage of 15 kV. The EDS was acquired in area mode.

2.3.8 X-ray diffraction spectroscopy. A powder X-ray diffractometer (PANalytical Empyrean) was used to determine the shift in peak intensities and *d*-spacing in the biocarbon samples. The effects of carbonization temperature on the *d*-spacing of the biocarbon samples that may represent relaxation and stress or contraction and expansion between the planes of atoms were studied. The 'reflection-transmission spinner' configuration was used for examining the samples in continuous scan mode. The analysis was conducted at tension 45 kV and 40 mA current setting of the X-ray generator. The samples were scanned from 5 to 80° to obtain diffractograms. The *d*-spacing was determined using HighScore Plus software.

2.3.9 Electrical conductivity. The electrical resistance of the burlap biocarbon pyrolyzed at various temperatures was determined using an Autolab PGSTAT302N coupled with FRA32 M impedance analysis module. Dried (at 105 °C) biocarbon samples were used before analysis. For each test, 300 mg of the samples was filled in a hollow cylindrical bar of 10 mm internal diameter. Aluminum pistons that acted as the anode and cathode were used to sandwich the biocarbon. Alligator clips were attached to the piston setup to complete the circuit between the electrodes and the Autolab machine. The current was generated by maintaining a 10 mV voltage difference and a 400–600 kHz frequency range. The compression pressure was increased during the test from 124.84 to 1123.57 kPa by putting the 1, 3, 5, 7, and 9 kg loads. The conductivity of the samples was calculated using Pouillet's law (eqn (2)):

$$\sigma = L/RA \quad (2)$$

where σ represents the electrical conductivity (S cm^{-1}) and L, R and A are the height of the biocarbon column (cm), resistance detected by the instrument (Ohm) and the base area of the hollow cylinder (cm^2), respectively. The conductivity was checked five times at each compression pressure, and the average with standard deviation is shown in the graph. Furthermore, to check the effect of maximum pressure (9 kg load) used in electrical conductivity, analyses such as SEM, XRD and BET were conducted for the pyrolyzed biocarbon at 1000 °C. The SEM, XRD and BET results (uncompressed *vs.* compressed) were compared and are mentioned in Fig. S1, S2 and Table S1, respectively, in the ESI.†

3. Results and discussion

3.1 Burlap biocarbon yield

The yield of biocarbon obtained on pyrolyzing burlap biomass was determined using eqn (1). Fig. 2 illustrates that with an increment in the carbonization temperature (from 325 °C to 1000 °C), the yield decreases from 71 to 22 wt%. It signifies that as the carbonization temperature increases, the cleavage of bonds and functional groups present in the lignocellulosic burlap biomass increases. A continuous decrease in the biocarbon yield in the range of 325–700 °C indicates the decomposition or breakdown of hemicellulose, cellulose and lignin present in the lignocellulosic biomass.[32] During pyrolysis at higher temperatures, devolatilization and thermal cracking occurred in the biomass. Similar observations of a decrease in biocarbon yields with an increase in carbonization temperatures were also observed by Chen *et al.*;[33] Zhao *et al.*[20] and Paleri *et al.*[22] It was further observed that there is a negligible change in yield beyond 600–700 °C pyrolysis temperature that became constant at pyrolysis temperatures of 800–1000 °C (*i.e.*, the yield remains ~22 wt%). The no change in yield at higher temperatures reveals that all the volatiles in the lignocellulosic burlap biomass were removed before 800 °C, and the higher stable aromatic component remained.

3.2 Effect of carbonization temperature on the functionality

The FTIR analysis was conducted to analyse the influence of the carbonization temperature on the functionality of burlap biomass (Fig. 3).

The broad peak at 3335 cm^{-1} present in GBF signifies the stretching vibrations of the hydroxyl (O–H) group. The peaks at 2919 and 2851 cm^{-1} denote the existence of symmetric and

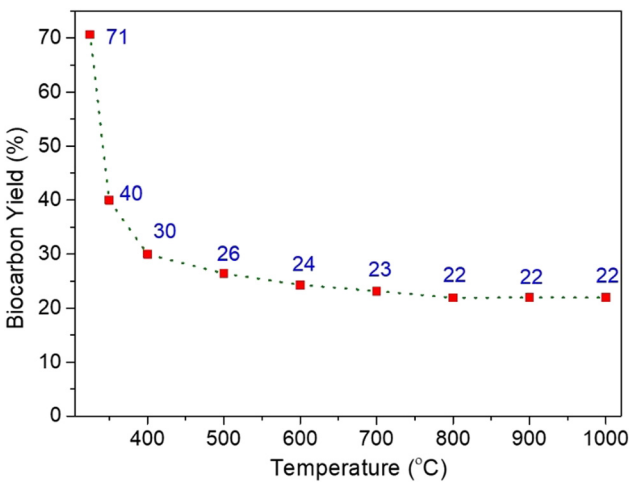

Fig. 2 Burlap biocarbon yield after carbonization at different temperatures.

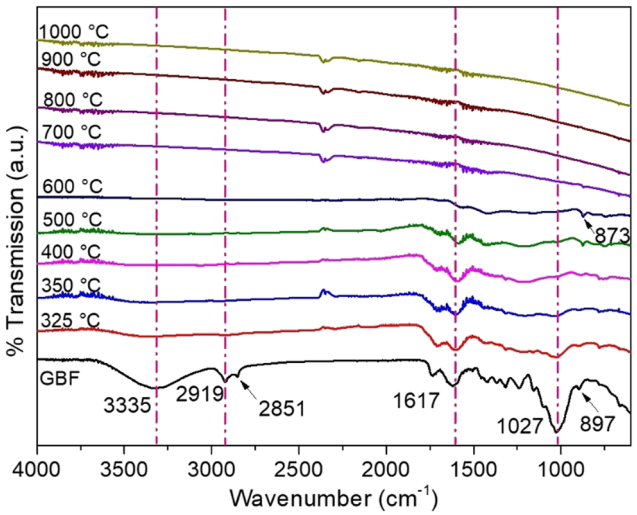

Fig. 3 FTIR spectra of the burlap biocarbon samples carbonized at different temperatures.

asymmetric C–H stretching on aliphatic hydrocarbons (alkane stretch) and symmetric stretch, respectively, present in lignocellulosic constituents. The peak at 1617 cm^{-1} represents the C═O stretching present in cellulose-hemicellulose and the C═C aromatic bond present in lignin. In addition to that, the peaks at 873 and 897 cm^{-1} represent aromatic out-of-plane bending vibrations due to ring substitution.[34–36]

From the FTIR spectra, it can be observed that with the rise in carbonization temperature, the peak intensity reduces, indicating the loss of volatiles and components present in the lignocellulosic part that is degradable at low carbonization temperatures. The presence of functional groups until 600 °C carbonization temperature represents the functionality of lignin retained in the biocarbon up to 600 °C. Beyond the 600 °C pyrolysis temperature, the functionality of the biocarbon was not retained as the peaks that indicate the presence of hemicellulose, cellulose and lignin were not visible. Furthermore, it was noted that the peaks representing aromatic signals (873 cm^{-1}) retained at around 600 °C show the presence of lignin (as lignin-containing aromatic rings have a higher thermal stability than cellulose-hemicellulose). The change in functionality was supported by the percent yield obtained after the carbonization of burlap biomass.

3.3 Effect of carbonization temperature on the thermal stability and ash content

The thermal stability of the biocarbon samples was checked using the analysis (Fig. 4). The derivative graph shows that the peak height reduces with an increase in the pyrolysis temperature. The derivative weight curves (%/°C) demonstrated that the maximum peak height shifts towards a higher temperature with an increase in carbonization temperature due to the prior carbonization in the pyrolizer.[22]

In addition to that, with an enhancement in the carbonization temperature, the weight percent rate of the samples decreases. The change in weight percent rate was significant

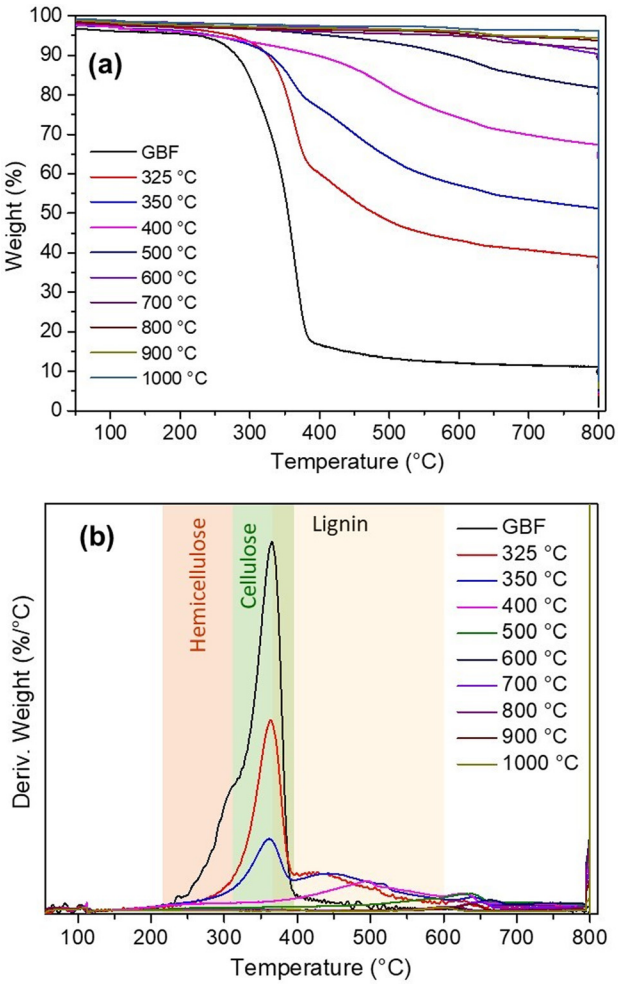

Fig. 4 Thermal stability of burlap biomass and its biocarbon yield after carbonization at different temperatures (the colored region represents the degradation range of the hemicellulose, cellulose and lignin): (a) weight % *vs.* temperature; (b) deriv. weight *vs.* temperature.

up to 600 °C and beyond 600 °C, less change was observed. This increased thermal stability reveals that all the volatiles in the lignocellulosic biomass were removed at around 600 °C (also proved by the percent yield of biocarbon and FTIR analysis), and the higher stable aromatic component remained. Hence, it can be concluded that the thermostability of the biocarbon samples increases when the carbonization temperature is increased from 325 to 1000 °C.

A similar behaviour of biochar was observed by Ma *et al.*[37] Yang *et al.*[38] studied the degradation temperature range of commercial cellulose, hemicellulose and lignin. It was noted that the degradation of hemicellulose resulted in the range of 220–315 °C, while that of cellulose occurred at 315–400 °C. However, lignin decomposes in a wide range, and its range depends on the type of lignin (based on the origin and extraction process). The lignin depolymerization starts with the cleavage of H_2 and C–OH (weaker bonds), followed by β-O-4 bonds at higher temperatures.[6] Brebu *et al.*[39] stated that the maximum degradation range was around 370–385 °C; however, mass loss continued above 550 °C slowly due to aromatic condensation. Bartkowiak *et al.*[40] stated that up to 600 °C, mass loss of lignin is still retained.

Table 1 Physicochemical properties of burlap biocarbon carbonized at different temperatures

Burlap biomass carbonization temperature (°C)	TGA	BET	XRD	
	Ash content (wt%)	Surface area (m^2 g^{-1})	Peak position (2θ)	d-spacing (Å)
325	3.29 ± 1.12	2.902	24.3	3.66
350	3.81 ± 1.13	3.297	24.32	3.66
400	4.9 ± 0.03	4.120	24.38	3.65
500	5.34 ± 0.27	6.126	29.33	3.05
600	6.21 ± 1.26	31.965	29.41	3.04
700	6.08 ± 1.03	87.914	29.38	3.04
800	6.7 ± 0.62	39.323	31.32	2.86
900	6.62 ± 1.27	11.193	31.33	2.86
1000	7.59 ± 0.03	7.265	31.34	2.85

The mass loss rate in the case of lignin was the slowest.[38] Furthermore, it was noted that the ash content increases with an increase in the carbonization temperature (shown in Table 1). The increment in ash content occurred due to the progressive concentration of inorganic mineral constituents (K, Ca, and Si).[41,42] The change in thermal stability of burlap biocarbon was affirmed by the percent yield and the presence of functional groups in burlap biocarbon at different temperatures (325–1000 °C).

3.4 Effect of carbonization temperature on the functionality of the evolved gaseous residues

The analysis was conducted to determine the release of gases from the biocarbon samples during heating (up to 900 °C in a TGA instrument in an inert atmosphere). The analysis helps in detecting residues that evolve in the form of gases during thermal decomposition. The analysis also provides information on the environmental impact during pyrolysis.[35] Fig. 5 shows the 3D spectra of gaseous products produced from burlap fibers and burlap biocarbon samples. The burlap (jute) biomass comprises cellulose, hemicellulose and lignin.[31] Fig. 5(a) shows the removal of volatile organic compounds from burlap fibers in a wide range of temperatures. The gaseous compounds are alcohols (methanol and ethanol), acetone, acetaldehyde and phenol derivatives.[6] Among all the three components, lignin is highly thermally stable as it exhibits the evolution of gases up to a higher temperature relative to the hemicellulose and cellulose, and for a wider temperature range.[37,43] The decomposition temperatures of cellulose and hemicellulose are less than that of lignin. Lignin consists of aromatic rings in each structural unit with different reactivities, resulting in a milder mass loss or decomposition.[33] The absorption peak of products at 3800–3500 cm^{-1} represents H_2O, 3100–2800 cm^{-1} represents CH_4, 2390–2250 cm^{-1} represents CO_2, and 2240–2040 cm^{-1} represents CO. Hence, a wider pyrolysis temperature range was noted for lignin than cellulose and hemicellulose.

The absorption band (2390–2250 cm^{-1}) indicates that with an increase in the carbonization temperature, the CO_2 intensity reduces. The reduced intensity could be observed due to the conversion of unstable to more thermally stable biocarbon as the pyrolysis temperature increases; hence, the susceptibility to thermal decomposition reduces.

3.5 Effect of carbonization temperature on the disordered and graphitic (ordered) carbon

Raman scattering analysis was conducted to determine the D- and G-band ratio. The D-band resulted due to turbostratic carbon,[44] representing disordered and distorted carbon, and the G-band represents highly ordered or graphitic carbon.[45]

The intensity ratio (I_D/I_G) of the two (D and G) bands was calculated by taking the ratio of the amplitude height of the deconvoluted peaks at Raman shift 1300–1400 cm^{-1} for D and 1500–1600 cm^{-1} for G peaks.[44] Fig. 6 illustrates that with the rise in pyrolysis temperature (from 500–1000 °C), the intensity ratio (I_D/I_G) increases (I_D/I_G values are shown in Fig. 6). Thus, it signifies that the disordered structure increases with an increase in the pyrolysis temperature.

Furthermore, the crystallite size (L_a) (nm) of the biocarbon samples was calculated using eqn (3):

$$L_a = (2.4 \times 10^{-10})\lambda^4(I_D/I_G)^{-1} \quad (3)$$

where λ is the incident laser wavelength (nm) and I_D/I_G is the D and G band intensity ratio (unitless).[44,46]

The calculated crystal size value for 500, 600, 700, 800, 900 and 1000 °C were 36.97, 20.46, 18.49, 16.16, 16.03 and 16.03 nm, respectively. A decrease in the crystallite size with an increase in carbonization temperature was observed. Snowdon *et al.*[44] also observed an increase in the I_D/I_G ratio with a rise in carbonization temperatures.

3.6 Effect of carbonization temperature on the surface area of the burlap biocarbon

BET analysis was performed for the carbonized burlap biomass. The change in the specific surface area of burlap biocarbon with a change in carbonization temperature is shown in Table 1. It was observed that the surface area was enhanced when burlap biomass was carbonized from 325 to 700 °C. Furthermore, the specific surface area was reduced with a rise in carbonization temperature from 700 to 1000 °C. The enhancement of surface area from 325 to 700 °C was 30.3%, and the reduction from 700 to 1000 °C was 12%. The increase in the surface area occurred because of the accelerated release of volatile matter, resulting in complete devolatilization. After the complete decomposition of hemicellulose, the cellulose resulted in an enhanced surface area as cellulose microfibrils controlled the dimensional modifications.[47] The rise in carbonization temperature to 700 °C also results in pore enlargement. However, the increment above 700 °C leads to a decrease in surface area. The decrease in surface area was observed due to the collapse of internal structures of biocarbon (adjacent walls breakdown because of the pore enlargement), resulting in a decline in surface area. A similar decrease in surface area with an increase in pyrolysis temperature was also observed by Elnour *et al.*[48] and Dhar *et al.*[47]

3.7 Effect of carbonization temperature on the surface morphology and percent carbon content

SEM was conducted to determine the surface morphology of the biocarbon samples (Fig. 7) and identify their microstructure.

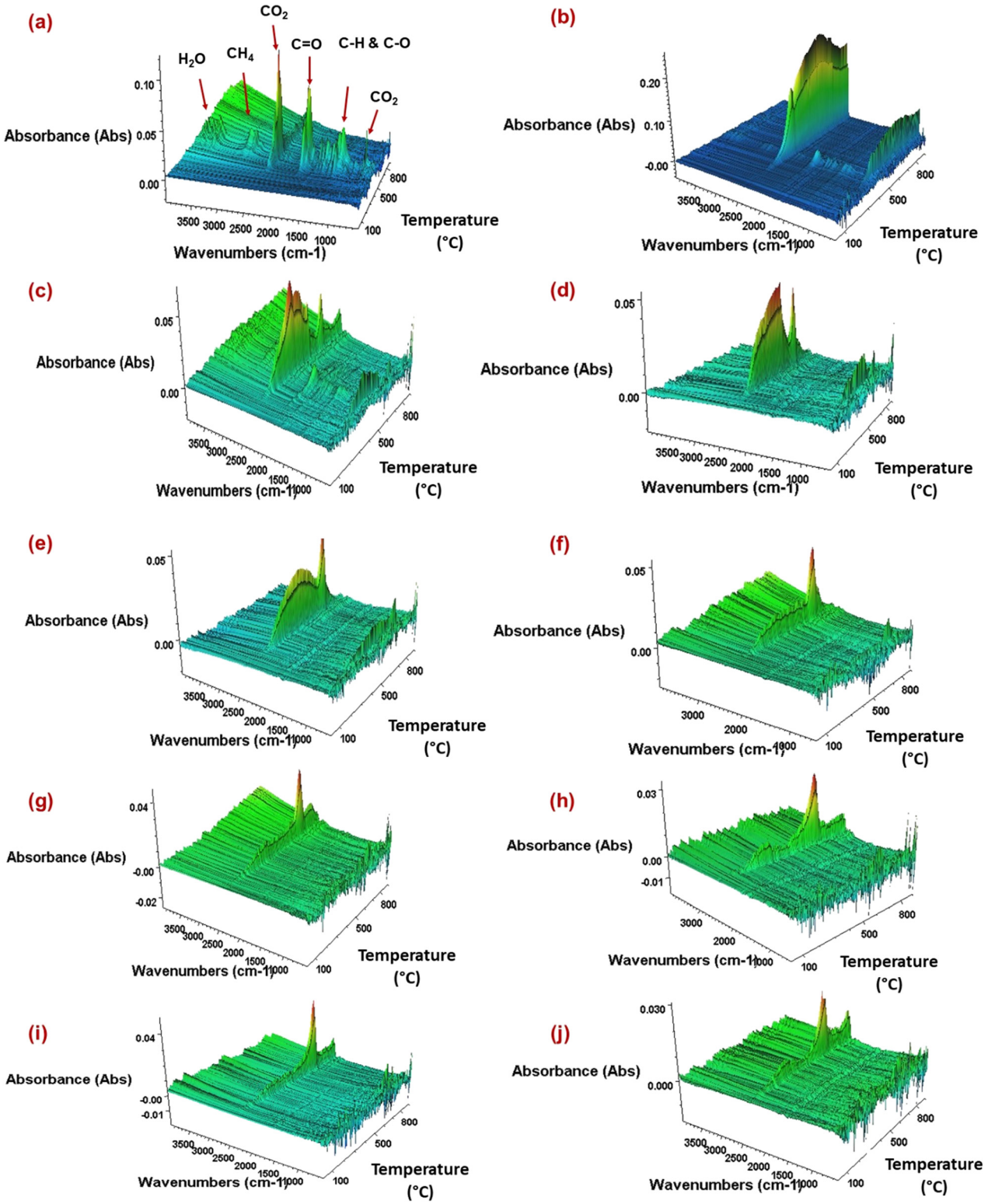

Fig. 5 TGA-FTIR 3D spectra of (a) ground burlap fibers (BF); pyrolyzed at (b) 325 °C, (c) 350 °C, (d) 400 °C, (e) 500 °C, (f) 600 °C, (g) 700 °C, (h) 800 °C, (i) 900 °C, and (j) 1000 °C.

EDS helped in determining the percent of carbon and oxygen present in the samples (Fig. 8).

The biocarbon pyrolyzed at 600 °C (Fig. 7(e)) and 700 °C (Fig. 7(f)) demonstrated larger sizes than lower carbonization temperatures (325–500 °C). The increase in particle size at 600 °C was also observed by Li *et al.*[49] Furthermore, the biocarbon pyrolyzed at 600 °C and 700 °C showed a lotus root-like morphology. The porous morphology was obtained

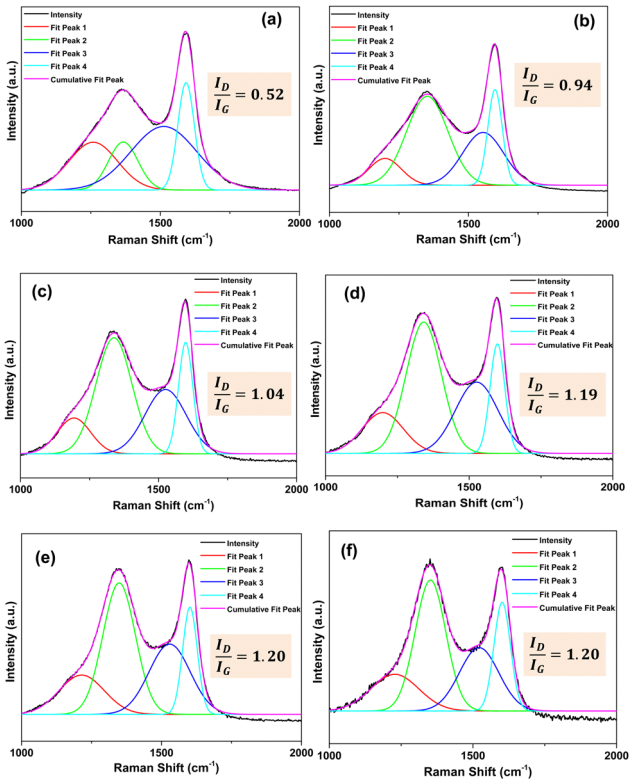

Fig. 6 Deconvoluted Raman spectra of burlap biocarbon pyrolyzed at (a) 500 °C, (b) 600 °C, (c) 700 °C, (d) 800 °C, (e) 900 °C, and (f) 1000 °C.

due to the dislodging of organic volatiles. A similar morphology was also observed by Chen *et al.*[50] Som *et al.*[51] also evidenced

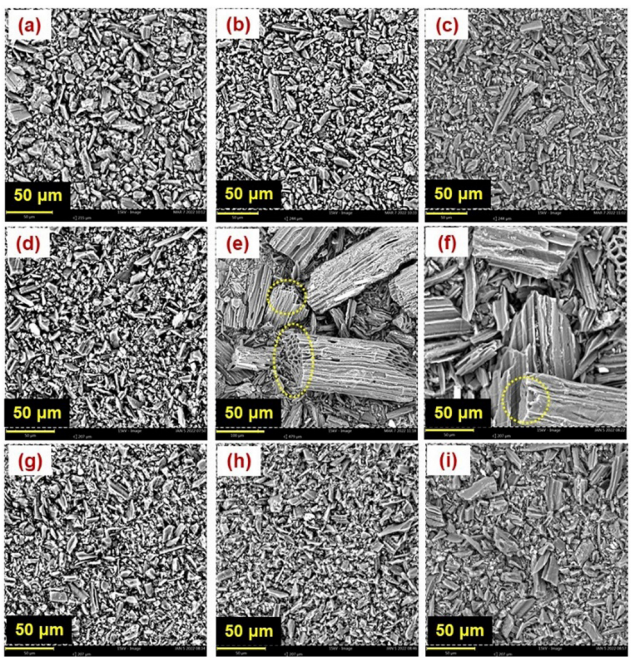

Fig. 7 Surface morphology of the burlap biocarbon pyrolyzed at (a) 325 °C, (b) 350 °C, (c) 400 °C, (d) 500 °C, (e) 600 °C, (f) 700 °C, (g) 800 °C, (h) 900 °C, and (i) 1000 °C.

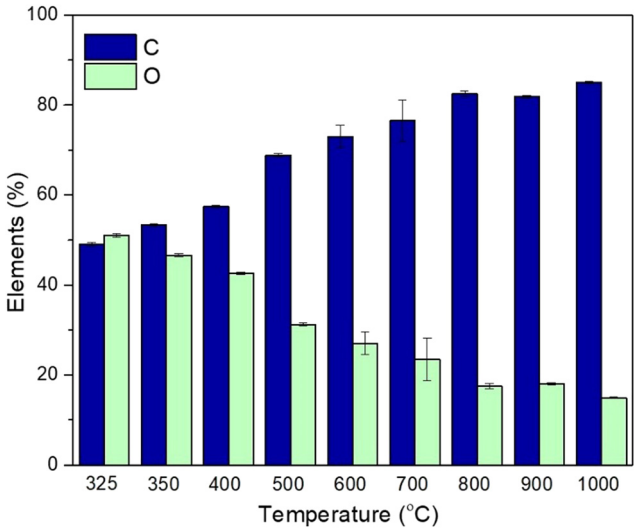

Fig. 8 SEM-EDS of the burlap biocarbon pyrolyzed at 325 °C, 350 °C, 400 °C, 500 °C, 600 °C, 700 °C, 800 °C, 900 °C, and 1000 °C.

the existence of this morphology after pyrolysis of palm frond and stated the occurrence because the lignin fused and formed pores during pyrolysis.

The increased porosity at a temperature of 600 °C is due to the quick release of gases during lignin decomposition that was retained at 700 °C.[42] Fig. 8 shows the effect of pyrolysis temperature on the elemental composition.

It was observed that with rise in pyrolysis temperature from 325 to 1000 °C, carbon content increased from 49 to 85%; however, oxygen content reduced from 51 to 15%. The higher carbon content at a higher pyrolysis temperature resulted in the formation of fixed carbon by depolymerization of lignocellulose. During the process, labile components such as oxygen and hydrogen were removed by dehydration and deoxygenation. This behavior was also evidenced by Zhao *et al.*[20] In addition to that, less oxygen component in biocarbon signifies its higher stability as oxygen renders a reaction that leads to degradation.

3.8 Effect of carbonization temperature on the interlayer spacing of burlap biocarbon

XRD analysis was conducted to determine the crystalline and amorphous phases present in the biocarbon samples (Fig. 9). The interlayer *d*-spacing between the burlap biocarbon layers was also detected (Table 1). Fig. 9(a) shows the high intensity, sharp narrow peak (at 2θ = 26.61°) of a commercial graphite sample with a *d*-spacing of 3.35 Å, demonstrating its crystalline nature. It implies that commercial graphite is a highly oriented carbon material and has a crystalline structure. However, the burlap biomass carbonized from 325–1000 °C shows an amorphous nature (randomly distributed atoms). The shift of peak towards a higher 2θ angle (Fig. 9(b)) signifies that the increase in carbonization temperature resulted in compressive stresses between the carbon layers. The reduced *d*-spacing was also validated by the analysis. The *d*-spacing for 325 °C was 3.66 Å, which was reduced to 2.85 Å for 1000 °C burlap biocarbon

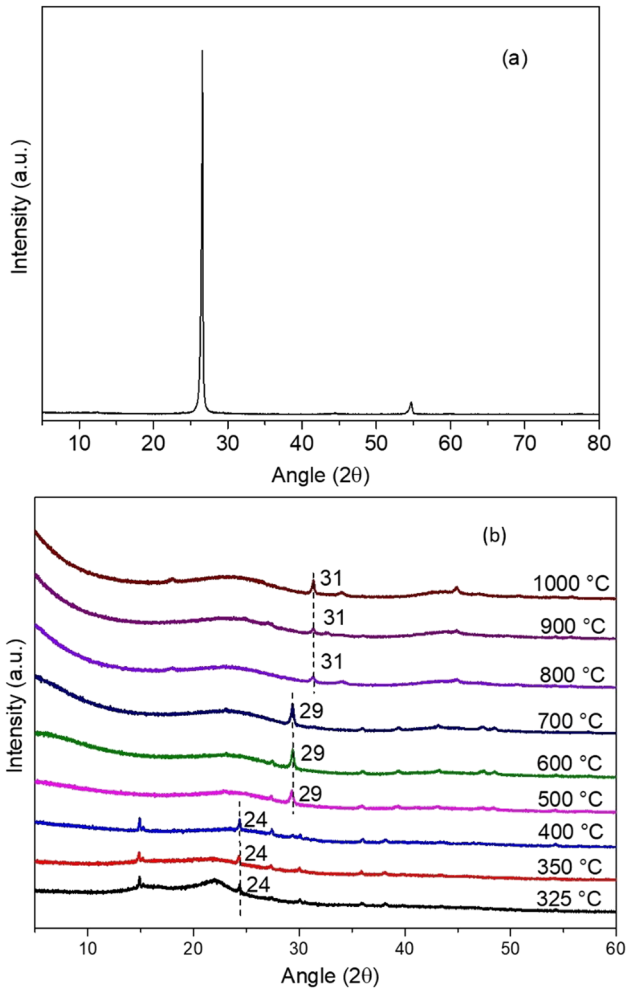

Fig. 9 XRD spectra of (a) commercial graphite and (b) burlap biocarbon samples carbonized at different temperatures.

(Table 1). Li *et al.*[49] also observed that as the pyrolysis temperature was increased, the interlayer *d*-spacing reduced.

3.9 Effect of carbonization temperature on the electrical conductivity

Nowadays, there is a significant requirement to develop a low-cost ubiquitous biographite that can be used to enhance modulus in polymer composites and energy storage applications. It is critically essential to discover and develop carbon obtained from waste biomass with a significantly higher conductivity. Biographite will also decrease the dependence on fossil-based resources.

The increase in the electrical conductivity was viewed with an increase in pressure loadings due to a decrease in the volume of samples resulting in close packing of the powder particles (Fig. 10). A similar behavior was observed for graphene samples. The lower compression pressure was insufficient to achieve the full potential of the samples showing electrical conductivity. The lowest conductivity was observed at 124.84 kPa because of the presence of air gaps between the particles.

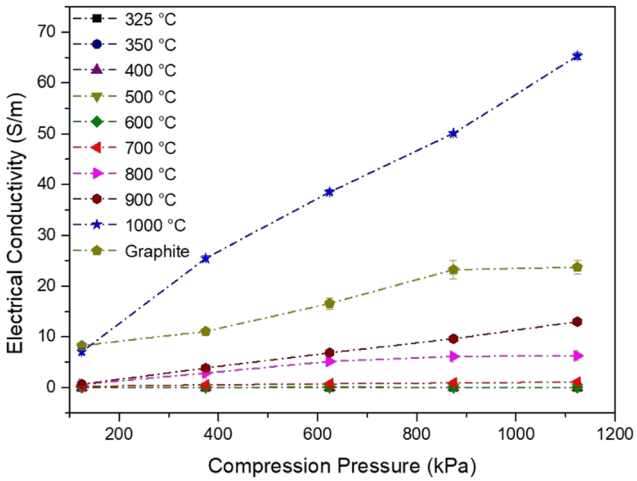

Fig. 10 Effect of electrical conductivity of burlap biocarbon on varying compression pressure and carbonization temperature at (a) 325 °C, (b) 350 °C, (c) 400 °C, (d) 500 °C, (e) 600 °C, (f) 700 °C, (g) 800 °C, (h) 900 °C, and (i) 1000 °C.

Moreover, as the gap decreases, electrical conductivity increases.

Kane *et al.*[52] compared the physicochemical properties of biochar obtained by pyrolyzing lignin at 900 and 1100 °C. The laboratory isolated lignin showed an electrical conductivity of 18.5 S cm^{-1} and further suggested meticulously tailoring biochar properties.

The significant enhancement of electrical conductivity for the biocarbon samples was observed even though the sample was amorphous, unlike graphite/graphene, because the rise occurred due to the interconnected pores. BET analysis shows that the surface area first increases to 700 °C and decreases with a further rise in the carbonization temperature. A decline in the surface area occurred due to the collapse of walls of the biocarbon due to the enlargement of pores at 700 °C. These interconnected pores that may lead to intense packing make the movement of electrons easier.

In addition, the shift in the 2θ angle to a higher value occurred due to the compressive residual stress or contraction of the layers (also affirmed by the *d*-spacing value from XRD) developed in the sample as the carbonization temperature increased. Giorcelli *et al.*[53] also confirmed the enhancement in conductivity with an increase in pressure and stress on the samples.

4. Conclusions

The work probed the effect of carbonization (pyrolysis at low (torrefied) and at high temperatures) of waste burlap (jute) sustainable biocarbon on its physicochemical and electrical properties. The carbonization was conducted at 325, 350, 400, 500, 600, 700, 800, 900 and 1000 °C. The following observations were made:

- The biocarbon yield was 71–22 wt% when carbonized at 325–1000 °C. The change in yield was negligible (±1%) beyond

600 °C. The yield was constant (22 wt%) towards higher temperatures *i.e.*, 800, 900 and 1000 °C.

• The thermal stability increases with an increase in carbonization temperature.

• As the carbonization temperature increased, the highest peak at the diffraction angle shifted towards a higher angle, and the *d*-spacing also reduces with a rise in carbonization temperature, which signifies the contraction of layers leading to compressive residual stress generated at a higher carbonization temperature.

• SEM-EDS revealed that the maximum carbon content obtained was 85% on pyrolyzing burlap biomass at 1000 °C.

• The electrical conductivity of burlap biocarbon pyrolyzed at 1000 °C showed a 250% improvement compared with commercial graphite.

The results from the analyses corroborated the enhancement in electrical conductivity. Hence, the tuning of burlap biocarbon will further show excellent enhancement in electrical conductivity and have the potential to replace non-renewable graphite that needs a higher electrical conductivity for certain applications.

Author contributions

Methodology, investigation, data analysis, and writing – original draft preparation, N.T.; investigation, validation, and writing – review and editing, A. R. and H. W.; project conceptualization, methodology, administration, resources, funding acquisition and supervision, and writing – review and editing, A. K. M. and M. M.; all authors contributed to the discussion, reviews and approval of the manuscript for publication.

Conflicts of interest

There are no conflicts to declare.

Acknowledgements

The authors would like to thank the financial support of (i) the Ontario Research Fund, Research Excellence Program; Round 9 (ORF-RE09) Ontario Ministry of Economic Development, Job Creation and Trade (Project No. 053970 and 054345); (ii) the Ontario Agri-Food Innovation Alliance – Bioeconomy for Industrial Uses Research Program (Project No. 030331 and 030332); (iii) the Ontario Agri-Food Research Initiative (Project No. 055217); (iv) the Natural Sciences and Engineering Research Council (NSERC) – Collaborative Research and Development Grants (CRD) Project No. 401637 with the partner industries Prism Farms Limited and Competitive Green Technologies, Lamington, Ontario, Canada for carrying out this study. The authors would also like to thank Club Coffee, Ontario, Canada for the burlap samples; and the powder XRD data were collected at the Chemistry Department X-Ray Diffraction Facility, University of Guelph for the powder XRD study.

References

1 S. Yang, Y. Cheng, X. Xiao and H. Pang, Development and application of carbon fiber in batteries, *Chem. Eng. J.*, 2020, **384**, 123294.
2 Z. Zhao, P. Bai, W. Du, B. Liu, D. Pan and R. Das, *et al.*, An overview of graphene and its derivatives reinforced metal matrix composites: Preparation, properties and applications, *Carbon*, 2020, **170**, 302–326.
3 J. R. Werber, C. O. Osuji and M. Elimelech, Materials for next-generation desalination and water purification membranes, *Nat. Rev. Mater.*, 2016, **1**, 1–15.
4 K. Nekoueian, M. Amiri, M. Sillanpää, F. Marken, R. Boukherroub and S. Szunerits, Carbon-based quantum particles: An electroanalytical and biomedical perspective, *Chem. Soc. Rev.*, 2019, **48**(15), 4281.
5 K. M. Liew, M. F. Kai and L. W. Zhang, Carbon nanotube reinforced cementitious composites: An overview, *Composites, Part A*, 2016, **91**, 301–323.
6 M. Erfani Jazi, G. Narayanan, F. Aghabozorgi, B. Farajidizaji, A. Aghaei and M. A. Kamyabi, *et al.*, Structure, chemistry and physicochemistry of lignin for material functionalization, *SN Appl. Sci.*, 2019, **1**, 1–19.
7 X. You, M. Misra, S. Gregori and A. K. Mohanty, Preparation of an Electric Double Layer Capacitor (EDLC) Using Miscanthus-Derived Biocarbon, *ACS Sustainable Chem. Eng.*, 2018, **6**(1), 318–324.
8 E. Behazin, M. Misra and A. K. Mohanty, Sustainable biocarbon from pyrolyzed perennial grasses and their effects on impact modified polypropylene biocomposites, *Composites, Part B*, 2017, **118**, 116–124.
9 S. Meyer, B. Glaser and P. Quicker, Technical, economical, and climate-related aspects of biochar production technologies: A literature review, *Environ. Sci. Technol.*, 2011, **45**, 9473–9483.
10 B. P. Chang, A. K. Mohanty and M. Misra, Sustainable biocarbon as an alternative of traditional fillers for poly(butylene terephthalate)-based composites: Thermo-oxidative aging and durability, *J. Appl. Polym. Sci.*, 2019, **136**(27), 47722–47735.
11 N. Tripathi, M. Misra and A. K. Mohanty, Durable Polylactic Acid (PLA)-Based Sustainable Engineered Blends and Biocomposites: Recent Developments, Challenges, and Opportunities, *ACS Eng. Au*, 2021, **1**(1), 7–38.
12 A. K. Mohanty, S. Vivekanandhan, J. M. Pin and M. Misra, Composites from renewable and sustainable resources: Challenges and innovations, *Science*, 2018, **362**, 536–542.
13 N. A. Mohamad Aini, N. Othman, M. H. Hussin, K. Sahakaro and N. Hayeemasae, Effect of hybrid carbon black/lignin on rheological, mechanical and thermal stability properties of NR/BR composites, *Plast., Rubber Compos.*, 2021, 1–3.
14 B. Valle, A. Remiro, N. García-Gómez, A. G. Gayubo and J. Bilbao, Recent research progress on bio-oil conversion into bio-fuels and raw chemicals: a review, *J. Chem. Technol. Biotechnol.*, 2019, **94**, 670–689.
15 T. Cordero-Lanzac, J. Rodríguez-Mirasol, T. Cordero and J. Bilbao, Advances and challenges in the valorization of

bio-oil: Hydrodeoxygenation using carbon-supported catalysts, *Energy Fuels*, 2021, **35**, 17008–17031.
16 B. P. Chang, A. Rodriguez-Uribe, A. K. Mohanty and M. Misra, A comprehensive review of renewable and sustainable biosourced carbon through pyrolysis in biocomposites uses: Current development and future opportunity, *Renewable Sustainable Energy Rev.*, 2021, **152**, 111666.
17 M. F. Adesemuyi, M. A. Adebayo, A. O. Akinola, E. F. Olasehinde, K. A. Adewole and L. Lajide, Preparation and characterisation of biochars from elephant grass and their utilisation for aqueous nitrate removal: Effect of pyrolysis temperature, *J. Environ. Chem. Eng*, 2020, **8**(6), 104507.
18 A. K. Varma and P. Mondal, Pyrolysis of sugarcane bagasse in semi batch reactor: Effects of process parameters on product yields and characterization of products, *Ind. Crops Prod.*, 2017, **95**, 704–717.
19 B. Zhao, H. Xu, T. Zhang, X. Nan and F. Ma, Effect of pyrolysis temperature on sulfur content, extractable fraction and release of sulfate in corn straw biochar, *RSC Adv.*, 2018, **8**(62), 35611.
20 B. Zhao, D. O'Connor, J. Zhang, T. Peng, Z. Shen and D. C. W. Tsang, *et al.*, Effect of pyrolysis temperature, heating rate, and residence time on rapeseed stem derived biochar, *J. Cleaner Prod.*, 2018, **174**, 977–987.
21 C. Zhao, X. Liu, A. Chen, J. Chen, W. Lv and X. Liu, Characteristics evaluation of bio-char produced by pyrolysis from waste hazelnut shell at various temperatures, *Energy Sources, Part A*, 2020, 1–11, DOI: 10.1080/15567036.2020.1754530.
22 D. M. Paleri, A. Rodriguez-Uribe, M. Misra and A. K. Mohanty, Pyrolyzed biomass from corn ethanol industry coproduct and their polypropylene-based composites: Effect of heat treatment temperature on performance of the biocomposites, *Composites, Part B*, 2021, **215**, 108714.
23 B. Li, L. Zhao, X. Xie, D. Lin, H. Xu and S. Wang, *et al.*, Volatile-char interactions during biomass pyrolysis: Effect of char preparation temperature, *Energy*, 2021, **215**, 119189.
24 W. Qu, J. Yang, X. Sun, X. Bai, H. Jin and M. Zhang, Towards producing high-quality lignin-based carbon fibers: A review of crucial factors affecting lignin properties and conversion techniques, *Int. J. Biol. Macromol.*, 2021, **189:**, 768–784.
25 H. Singh, J. I. P. Singh, S. Singh, V. Dhawan and S. K. Tiwari, A Brief Review of Jute Fibre and Its Composites, *Mater. Today: Proc.*, 2018, 28427–28437.
26 M. Ramachandran, S. Bansal and P. Raichurkar, Scrutiny of jute fiber poly-lactic acid (PLA) resin reinforced polymeric composite, *J. Text. Assoc.*, 2016, **76**(6), 372–375.
27 J. Gassan and A. K. Bledzki, Thermal degradation of flax and jute fibers, *J. Appl. Polym. Sci.*, 2001, **82**(6), 1417–1422.
28 X. Zhong, R. Li, Z. Wang, Y. Wang, W. Wang and D. Yu, Highly flexible, transparent film prepared by upcycle of wasted jute fabrics with functional properties, *Process Saf. Environ. Prot.*, 2021, **146**, 718–725.
29 L. Benhamadouche, M. Rokbi, H. Osmani, M. Jawaid, M. Asim and A. B. M. Supian, *et al.*, Characterization of physical and mechanical properties of recycled jute fabric reinforced polypropylene composites, *Polym. Compos.*, 2021, **42**(10), 5435–5444.
30 N. D. Choudhury, R. S. Chutia, T. Bhaskar and R. Kataki, Pyrolysis of jute dust: Effect of reaction parameters and analysis of products, *J. Mater. Cycles Waste Manage.*, 2014, **16**(3), 449–459.
31 W. W. Ming, C. Z. Sheng, Y. J. Yong and X. Z. Peng, Changes in composition, structure, and properties of jute fibers after chemical treatments, *Fibers Polym.*, 2009, **10**(6), 776–780.
32 K. Crombie, O. Mašek, S. P. Sohi, P. Brownsort and A. Cross, The effect of pyrolysis conditions on biochar stability as determined by three methods, *GCB Bioenergy*, 2013, **5**(2), 122–131.
33 D. Chen, X. Yu, C. Song, X. Pang, J. Huang and Y. Li, Effect of pyrolysis temperature on the chemical oxidation stability of bamboo biochar, *Bioresour. Technol.*, 2016, **218**, 1303–1306.
34 P. Quosai, A. Anstey, A. K. Mohanty and M. Misra, Characterization of biocarbon generated by high- and low-temperature pyrolysis of soy hulls and coffee chaff: For polymer composite applications, *R. Soc. Open Sci.*, 2018, **5**(8), 171970.
35 M. Picard, S. Thakur, M. Misra, D. F. Mielewski and A. K. Mohanty, Biocarbon from peanut hulls and their green composites with biobased poly(trimethylene terephthalate) (PTT), *Sci. Rep.*, 2020, **10**(1), 3310.
36 D. L. Pavia, G. M. Lampman, G. S. Kriz and J. A. Vyvyan, *Introduction to spectroscopy*, Cengage Learning, 2008.
37 Z. Ma, Y. Yang, Y. Wu, J. Xu, H. Peng and X. Liu, *et al.*, In-depth comparison of the physicochemical characteristics of bio-char derived from biomass pseudo components: Hemicellulose, cellulose, and lignin, *J. Anal. Appl. Pyrolysis*, 2019, **140**, 195–204.
38 H. Yang, R. Yan, H. Chen, D. H. Lee and C. Zheng, Characteristics of hemicellulose, cellulose and lignin pyrolysis, *Fuel*, 2007, **86**(12–13), 1781–1788.
39 M. Brebu, T. Tamminen and I. Spiridon, Thermal degradation of various lignins by TG-MS/FTIR and Py-GC-MS, *J. Anal. Appl. Pyrolysis*, 2013, **104**, 531–539.
40 M. Bartkowiak and R. Zakrzewski, Thermal degradation of lignins isolated from wood, *J. Therm. Anal. Calorim.*, 2004, 295–304.
41 A. Phounglamcheik, R. Vila, N. Kienzl, L. Wang, A. Hedayati and M. Broström, *et al.*, CO2 Gasification Reactivity of Char from High-Ash Biomass, *ACS Omega*, 2021, **6**(49), 34115–34128.
42 A. Tomczyk, Z. Sokołowska and P. Boguta, Biochar physicochemical properties: pyrolysis temperature and feedstock kind effects, *Rev. Environ. Sci. Bio/Technol.*, 2020, **19**, 191–215.
43 X. Cao, L. Zhong, X. Peng, S. Sun, S. Li and S. Liu, *et al.*, Comparative study of the pyrolysis of lignocellulose and its major components: Characterization and overall distribution of their biochars and volatiles, *Bioresour. Technol.*, 2014, **155**, 21–27.
44 M. R. Snowdon, A. K. Mohanty and M. Misra, A study of carbonized lignin as an alternative to carbon black, *ACS Sustainable Chem. Eng.*, 2014, **2**(5), 1257–1263.
45 T. Balint, B. P. Chang, A. K. Mohanty and M. Misra, Underutilized agricultural co-product as a sustainable biofiller for

polyamide 6,6: Effect of carbonization temperature, *Molecules*, 2020, **25**(6), 1455.

46 A. Ferrari and J. Robertson, Interpretation of Raman spectra of disordered and amorphous carbon, *Phys. Rev. B: Condens. Matter Mater. Phys.*, 2000, **61**(20), 14095–14107.

47 S. A. Dhar, T. U. Sakib and L. N. Hilary, Effects of pyrolysis temperature on production and physicochemical characterization of biochar derived from coconut fiber biomass through slow pyrolysis process, *Biomass Convers. Biorefin.*, 2020, 1–17.

48 A. Y. Elnour, A. A. Alghyamah, H. M. Shaikh, A. M. Poulose, S. M. Al-Zahrani and A. Anis, *et al.*, Effect of pyrolysis temperature on biochar microstructural evolution, physicochemical characteristics, and its influence on biochar/polypropylene composites, *Appl. Sci.*, 2019, **9**(6), 1149.

49 Z. Li, C. Reimer, M. Picard, A. K. Mohanty and M. Misra, Characterization of Chicken Feather Biocarbon for Use in Sustainable Biocomposites, *Front Mater.*, 2020, **7**, 1–12.

50 M. Chen, C. Bao, D. Hu, X. Jin and Q. Huang, Facile and low-cost fabrication of ZnO/biochar nanocomposites from jute fibers for efficient and stable photodegradation of methylene blue dye, *J. Anal. Appl. Pyrolysis*, 2019, **139**, 319–332.

51 A. M. Som, Z. Wang and A. Al-Tabbaa, Palm frond biochar production and characterisation, *Earth Environ. Sci. Trans. R. Soc. Edinburgh*, 2012, 39–50.

52 S. Kane, R. Ulrich, A. Harrington, N. P. Stadie and C. Ryan, Physical and chemical mechanisms that influence the electrical conductivity of lignin-derived biochar, *Carbon Trends*, 2021, **5**, 100088.

53 M. Giorcelli, M. Bartoli, A. Sanginario, E. Padovano, C. Rosso and M. Rovere, *et al.*, High-Temperature Annealed Biochar as a Conductive Filler for the Production of Piezoresistive Materials for Energy Conversion Application, *ACS Appl. Electron. Mater*, 2021, **3**(2), 838–844.